Spatial variation of the current in grain boundary Josephson junctions

M. Carmody
*Materials Science and Engineering Department, Northwestern University, Evanston, Illinois 60208
and Materials Science Division and Science Technology Center for Superconductivity,
Argonne National Laboratory, Argonne, Illinois 60439*

B. H. Moeckly
Conductus, Inc., 969 West Maude Avenue, Sunnyvale, California 94086

K. L. Merkle
*Materials Science Division and Science Technology Center for Superconductivity,
Argonne National Laboratory, Argonne, Illinois 60439*

L. D. Marks
Materials Science and Engineering Department, Northwestern University, Evanston, Illinois 60208

The spatial variation of the current across the boundary in several $YBa_2Cu_3O_{7-x}$ grain boundary Josephson junctions was determined using direct methods. A phase retrieval algorithm was used to calculate the positional critical current density $J(x)$ from critical current versus applied magnetic field, $I_c(B)$, measurements. The current distributions were highly nonuniform along the length of the junctions. These measurements are consistent with existing filamentary grain boundary models, low temperature scanning microscopy studies, and laser scanning microscopy studies of high T_c grain boundaries. The very large scatter in the critical currents reported in the literature for grain boundaries of the same macroscopic geometry appear to be due to the underlying variations in local critical currents. © *2000 American Institute of Physics.* [S0021-8979(00)01905-8]

I. INTRODUCTION

Understanding the relationship between the microstructure and transport properties of Josephson junctions is one of the keys to manufacturing reproducible high quality junctions. However, there are few methods of obtaining local transport information across the boundary. Therefore, a direct comparison between local microstructure and local transport data has not been possible. Variations in the spatial distribution of the current $J(x)$ across the boundary can be estimated using low temperature scanning electron microscopy (LTSEM) and laser scanning microscopy (LSM).[1–5] These scanning techniques measure a voltage difference as a beam is rastered from point to point along the length of the boundary. The actual current distribution is not directly measured, rather the voltage difference due to the incident beam is measured along the boundary and then related to the local current variation. The spatial resolution of these scanning techniques is on the order of 1 μm. Consequently, meaningful data sets for these scanning techniques can only be obtained from rather wide junctions. Also, the limited point to point sensitivity of these techniques gives only a rough estimate of the current distribution since small local deviations in the current are averaged out in the signal. Moreover, only rather large deviations in the current across the boundary are measurable.

An alternate method that has been explored for determining the local current variations along the length of the boundary in Josephson junctions is by measuring the magnetic field response of the critical current. For small junctions (when the width $W < 4\lambda_J$, where λ_J is the Josephson

penetration depth), self-field effects are assumed to be negligible and thus the magnetic field along the length of the grain boundary can be considered constant. For these types of junctions, if the current-phase relationship is sinusoidal, the Fourier relationship of Eq. (1) can be used to represent the relationship between the critical current as a function of the applied magnetic field $I_c(B)$ and the current across the boundary as a function of the position along the length of the boundary.[6]

$$I_c(B) = \left| \int_{-\infty}^{\infty} J(x) \exp[i\phi(x)] dx \right|, \qquad (1)$$

where $\phi(x) = qx + \phi_0$ and $q = 2\pi DB/\Phi_0$ (B is the magnetic field applied perpendicular to the current direction, Φ_0 is defined as the superconducting flux quantum ($h/2e = 2.07 \times 10^{-7}$ G cm^2) and $D = \lambda_1 + \lambda_2 + d$ where d is the thickness of the barrier and λ the London penetration depth.

When the current distribution along the boundary is uniform, Eq. (1) simplifies to the familiar Fraunhofer diffraction pattern. Most high T_c junctions that have been studied in the literature show large deviations from the ideal Fraunhofer magnetic interference pattern of a uniform junction.[7–16] It is believed that many of these deviations are due to structural and stoichiometric inhomogeneities along the grain boundary.

Since $I_c(B)$ is the modulus of the Fourier transform of $J(x)$, in general it is not possible to directly calculate $J(x)$ from $I_c(B)$. An approach that has been used for obtaining spatial information about the current across the boundary
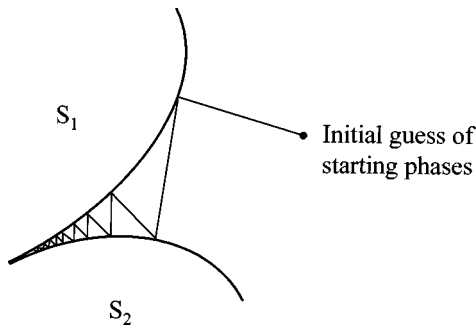
FIG. 1. Schematic diagram of projection between two convex constraint sets S_1 and S_2. Successive projections continue to converge towards a solution at the intersection of the two sets.

FIG. 2. Schematic diagram of a trap geometry. Set S_2 is a nonconvex set. Projection of an initial guess between the two sets may converge to a solution at the intersection of the two sets, but it can also lead to convergence at the trap which is not a solution. The point of convergence is dependent on the location of the starting guess.

using the Fourier relation of Eq. (1) is the calculation of the correlation function $C(x)$.[12–18] The correlation function $C(x)$ is

$$C(x) = \left| \int_{-\infty}^{\infty} |I_c(B)|^2 \exp[i\,\phi(x)]dx \right|, \qquad (2)$$

and has been used to analyze the spatial variation of the microstructure of the boundary.[12–18] Inverse Fourier transforming $I_c(B)$ to obtain the spatial variation of $J(x)$ requires knowledge of both the phase and the moduli. Equation (2) does not use any positional information regarding the inhomogenities of the current density. Therefore, the correlation function does not give direct positional information about the current across the boundary. Thus, the use of the correlation function does not allow for a direct comparison between current and the microstructure along the boundary.

　　Nesher and Ribak demonstrated that by using known constraints about the junction, in concert with existing phase retrieval algorithms it is possible to limit the number of possible solutions to the one-dimensional (1D) phase problem and restore $J(x)$ from $I_c(B)$.[19] In many cases a very small number of possible solutions exist and in some cases the solutions are unique.[19] Unfortunately, the rather easy task of restoring a set of missing phase information from a set of 1D moduli measurements is greatly complicated due to the nonconvex nature of the problem.[20] The general phase retrieval algorithm outlined by Nesher and Ribak can be formulated in set theoretic terms as the iterative projection of an initial guess between two constraint sets.[20] One constraint set is defined by the real space constraints (set S_1), and the other constraint set is defined by the Fourier space constraints (set S_2).[21] A correct solution is any solution that lies at the intersection of the two sets.[20] When both constraint sets are convex, all initial guesses at the solution will continue to converge to a possible correct solution.[20] Figure 1 is a schematic example of projection between two convex constraint sets S_1 and S_2. From Fig. 1, it is possible to see that projection back and forth between convex constraint sets will lead to a solution that is at the intersection of the two sets. However, it is well known that the Fourier constraint set for the 1D phase retrieval from modulus problem is not convex.[20] Consequently, there is no guarantee of convergence to a correct solution. Specifically, it has been demonstrated that traps and tunnels exist when projecting between two or more sets
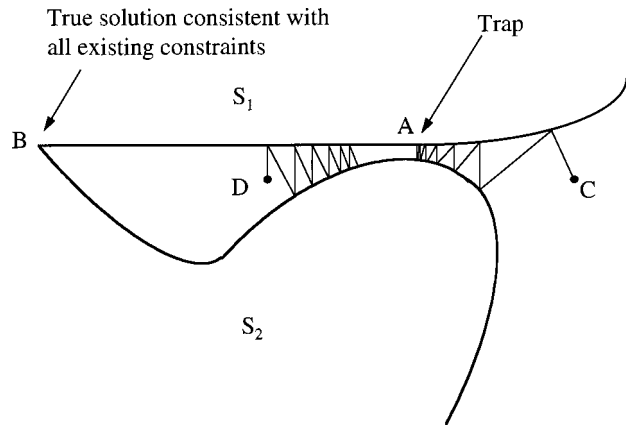
when at least one of the sets is nonconvex.[20] To illustrate this Fig. 2 shows an example of a possible trap geometry. From Fig. 2 it can be seen that an initial guess at or near point C or D would result in convergence to a trap at point A. Point A is not at the intersection of the two constraint sets and thus point A is not a solution. Figure 3 gives a schematic of a tunnel geometry. A tunnel may exist between the two constraint sets such that when projecting between the two sets the solution may stagnate far from an actual solution. Unlike the trap geometry, a solution that is caught in a tunnel will continue to converge towards a correct solution. However, due to the geometry of the tunnel, the convergence may proceed very slowly.

　　It is important to note that tunnel and trap solutions do not conform to the boundary constraints and should be discriminated against before evaluating possible correct solutions. A self-consistency check alone, as used by Nesher and Ribak, is not sufficient to determine convergence (if the last iteration of the algorithm is the same as the previous iteration) to a correct solution. In this case, it is possible to incorrectly conclude that the algorithm has converged to a solution when it is merely caught in a tunnel or a trap.

　　There are two important conclusions that can be drawn from the scenarios indicated by Figs. 2 and 3. First, the choice of the initial starting guess controls whether or not the algorithm will converge to a correct solution. Second, a rank-
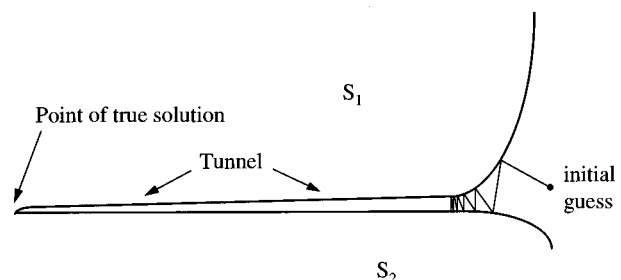

FIG. 3. Schematic diagram of a tunnel geometry. Tunnel geometry can lead to stagnation of the algorithm far from the intersection of the two sets depending on the proximity of the initial guess.

ing system or figure of merit (FOM) must be used to separate a starting guess that converges to a correct solution from a starting guess that converges to a tunnel or trap. Therefore, some of the starting guesses of a random number generator without the aid of a FOM will converge to tunnels and traps. Also, when testing various test models, specifically those with multiple correct solutions, we found that a random number generator has a very difficult time finding all possible correct solutions.

Understanding the above mentioned complexities, we have developed a phase retrieval algorithm that differs from the one used by Nesher and Ribak in two important aspects. One, we use a FOM to test whether a possible solution conforms to the known boundary constraints thus eliminating trap and tunnel solutions from consideration. Second, we use a genetic algorithm to effectively search solution space to find all possible solutions.

We have found that the most useful FOM for the 1D Josephson junction phase problem is one that checks whether or not the calculated solution conforms to the known boundary constraints after each iteration of the algorithm. We define our FOM as

$$\text{FOM} = \Sigma [I_c(B) - |F_i(B)|], \tag{3}$$

where $I_c(B)$ are the experimentally measured moduli and $|F_i(B)|$ is the calculated Fourier modulus of the ith iteration of the algorithm. When the algorithm converges to a possible correct solution at the intersection of the two constraint sets the FOM as we have defined it should be zero. When the algorithm converges to a trap or tunnel the FOM will be nonzero. In practice, slight errors in the data set will result in nonzero FOMs for correct solutions. However, we have found that the FOM for a correct solution is significantly smaller than the FOM of trap and tunnel solutions. Note that merely checking for convergence cannot distinguish between correct solutions and trap and tunnel solutions.

A genetic algorithm, is used to pick our starting sets of phases rather than a random number generator. The genetic algorithm ranks each of our solutions according to its FOM. Solutions that have a lower FOM are ranked as better solutions. The GA then selects a new starting point using preset parameters and the FOM information to pick new sets of phases more likely to conform to our known boundary constraints. Using the GA, the solutions continue to evolve and improve. Eventually, trap and tunnel solutions are eliminated due to their poor FOM and the top remaining solutions are all possible correct solutions. The details of this algorithm have been published previously.[21]

By using the above mentioned phase retrieval method to find the missing phase information and thus calculating $J(x)$, we are able to directly deduce the spatial variation of the current along the boundary. This provides the necessary means to correlate the variations in the current to variations in the microstructure along the boundary.

II. EXPERIMENTAL PROCEDURE

The high-angle grain boundary weak links that were studied were formed by depositing high-temperature super-

conducting [001] orientated thin films onto SrTiO$_3$ bicrystal substrates. The grain boundary misorientation angle about [001] was 24°. Our results were obtained using YBCO and Co-doped YBCO thin films. In the latter case, results are reported for total Co/Cu ratios of 0.01 and 0.02.

The films were grown by pulsed laser ablation to a thickness of about 250 nm. A CeO$_2$ buffer layer was employed to suppress a-axis-oriented growth. The pure YBCO films were grown at a substrate temperature of 780 °C and an oxygen pressure of 300 mTorr. The Co-doped films were grown at 800 °C and 800 mTorr. The films were patterned using Ar-ion etching to form microbridges spanning the grain boundary with widths of 1 to 10 μm. Magnetic field measurements were performed with the applied field parallel to the c axis (perpendicular to the substrate plane) in order to determine the response of the critical current.

III. CALCULATIONS

The $I_c(B)$ data sets were measured in both the positive and negative field directions. The $I_c(B)$ measurements were completely reversible with respect to field direction which is a requirement for this type of Fourier analysis. The current density $J(x)$ from Eq. (1) is assumed to be real. Therefore $I_c(B)$ must be symmetric about zero. Consequently, for calculation purposes, slight nonsymmetries in the $I_c(B)$ data were averaged out. There also existed in much of the data a residual current independent of the applied field which was subtracted out of the data before the algorithm was applied. The resolution of $J(x)$ in real space is determined by the magnetic field sweep. The spacing in real space between any two consecutive data points Δx is proportional to the inverse of the magnetic field sweep.

$$\Delta x = \frac{\Phi_0}{2\pi D \Delta B N}, \tag{4}$$

where ΔB is the magnetic field spacing, D is the same as from Eq. (1) and N is the total number of data points in the magnetic field sweep from $-B_{max}$ to B_{max}. The applied magnetic field values must be corrected for demagnetizing effects as pointed out by Rosenthal *et al.*[22] They suggested using an ellipsoidal approximation such that the aspect ratios of the boundary were identical to that of a thin flat spheroid. The resultant magnetic field would be enhanced by a factor of $\approx 1.2(W/t)$ where W is the junction width and t is the film thickness. This approximation has the advantage of being uniform across the boundary, however studies on the effect of the demagnetization geometry suggest that the approximation tends to overcompensate such that the calculated values are too large.[22–26] A demagnetization factor for a rectangular geometry identical to that of the boundaries used for examination was calculated based on the approach used by Joseph and Schlomann.[27] The demagnetization factor varies with position both along the width of the boundary as well as away from the boundary into the bulk of the sample by approximately 15%. For calculation purposes, the demagnetization factor in the z direction of the sample was averaged over the entire (x,y,z) range. The averaged demagnetization factors were approximately 50% smaller than those for a

TABLE I. The demagnetization factor D' for each sample using a rectangular geometry and a comparison of the rectangular value to the ellipsoidal value.

Boundary width	D' Ellipsoidal	Average D' rectangular
2 μm	~10.5	~4.9
5 μm	~25.53	~14.47

uniform flat ellipsoid disk with identical aspect ratios. Table I compares the calculated demagnetization factors for 2- and 5-μm-wide ellipsoidal and rectangular boundaries.

The phase retrieval algorithm produces solutions for $J(x)$ that are consistent with the known physical constraints on the boundary. Since the possibility exists for multiple solutions, we have used a genetic algorithm to rigorously search solution space for all possible solutions. When multiple solutions are identified we present all possible current distributions across the boundary.

IV. RESULTS AND DISCUSSION

All of the weak links investigated in the present study display clear Josephson behavior at low temperatures which is qualitatively well described by the resistively shunted junction model (excess current is very small). We obtain R_n values for these devices of several Ohms at 4.2 K, with I_c values ranging from several hundred mA to tens of μA as the Co concentration is increased. The Co is assumed to substitute for the Cu(1) atoms residing on the basal-plane Cu–O chains.[28] However, the transport properties of Co-doped YBCO films depends strongly on growth conditions.[28,29] It has been speculated that this is due to an inhomogeneous distribution of Co which varies with deposition parameters.[28] Films discussed here are surmised to have a relatively more homogeneous distribution of Co. The effect of Co doping on the Josephson properties of grain boundary properties is extensively discussed elsewhere.[29]

The calculated current distribution solutions for the devices showed similar results. Typically the algorithm found between one and three possible correct solutions. However, all of the solutions were similar, i.e., mathematically different but represented the same physical situation. Figure 4(a) is an example of a 5-μm-wide boundary $I_c(B)$ data set. Figure 4(b) shows two different solutions (lowest and identical FOM) that the phase retrieval algorithm found for the data set from part (a). The spatial resolution of the data points calculated from Eq. (4) correcting for the demagnetization field is $\approx$0.13 μm. There is a strong peak to peak correspondence between the solutions and the relative peak heights are similar. The two solutions found for the data set in Fig. 4 represent within the accuracy of the measurement the same current distribution. By contrast the solutions found by Nesher and Ribak did not have good correspondence between peak positions as well as relative peak heights. Different solutions would imply different physical distributions of the current along the boundary. Whenever multiple distinctly different solutions are mathematically possible, all solutions that conform to a zero FOM must be considered a possible
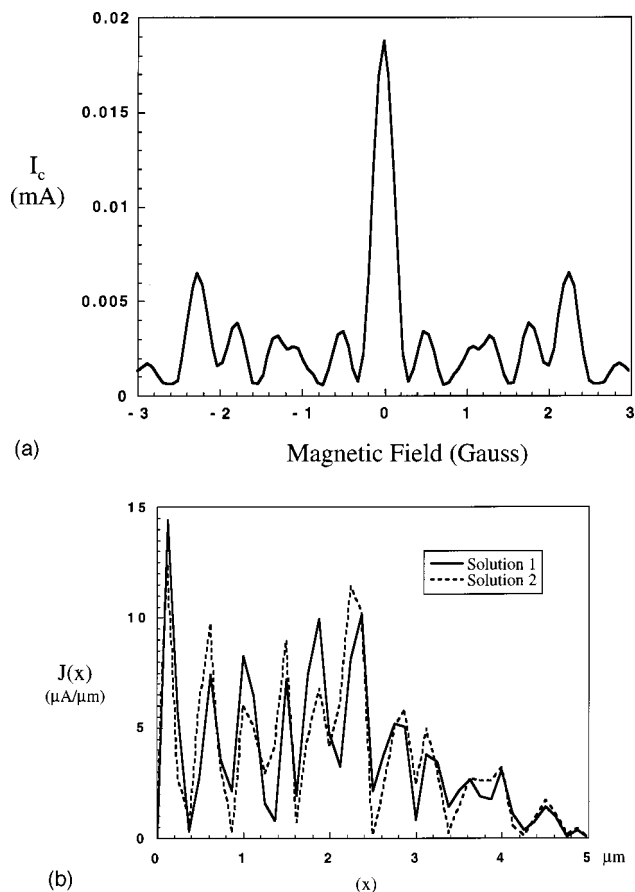

(a)

(b)

FIG. 4. (a) The critical current vs applied magnetic field profile for a 1% Co doped, 5 μm wide, 24° YBCO grain boundary junction used for calculation of the critical current density distribution. (b) Two critical current distributions $J(x)$ along the length of the boundary that the phase retrieval algorithm was able to determine. Note the close similarity between the two distributions.

correct solution. Thus it is extremely important to quantitatively rank the various solutions to determine which are actually correct solutions distinct from trap or tunnel solutions. The fact that the algorithm used here has always found just one type of solution within the accuracy of the experiment measurements and the validity of Eq. (1) indicates that our procedure is quite robust.

The general current behavior along the length of our boundaries is quite similar to the current variations reported by Nesher and Ribak. Notice how the current varies quite extensively from region to region along the length of the boundary in Fig. 4. Laser scanning microscopy imaging of the spatial variation of the critical current in high T_c grain boundaries has shown similar oscillations in the current along the length of the boundary.[4,5] However, due to the increased resolution and sensitivity of the present technique over LTSEM and LSM measurements, many of the calculated inhomogeneities of the current distribution would not be resolved by these scanning techniques and thus boundaries studied by these techniques would appear more uniform on a larger scale than the boundaries studied here.

Figure 5 shows a $I_c(B)$ data set of a second sample that was used for analyzing the spatial variation of the critical current. Figure 5(b) shows the calculated $J(x)$ distribution.
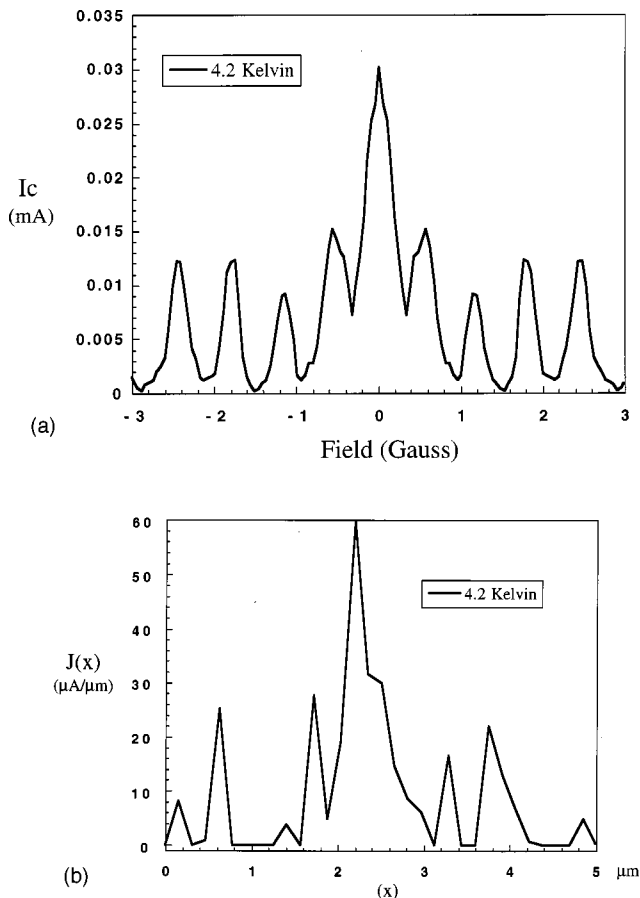
FIG. 5. (a) Critical current vs applied magnetic field for a 2.0% Co doped, 24°, 5 μm YBCO grain boundary junction used for calculation of $J(x)$ profiles. (b) $J(x)$ profile along the boundary calculated for the junction.

FIG. 6. Critical current vs applied magnetic field measurements for a 24° 5 μm YBCO grain boundary junction used for calculation of $J(x)$ profiles at (a) 4 and (b) 60 Kelvin.

All starting sets of phases converged to a single solution for this sample. Local current variations are similar to those found along the boundary of the sample from Fig. 4. Note that these solutions indicate that the majority of the current is carried by a small number of superconducting segments along the boundary separated by regions that carry little or no current. There have been several grain boundary models that suggest the current across the boundary is carried by a series of small (nanometer length scale) superconducting filaments along the length of the boundary.[30–35] Our results in no way contradict these models, however due to the limited magnetic field sweep of our data and the resulting lower resolution of the current distributions, we would expect our boundaries to appear more uniform than the microfilamentray models would suggest.

Figure 6 shows $I_c(B)$ data from a 5 μm boundary measured at two different temperatures. The positional current $J(x)$ across the boundary was calculated for each data set with a spatial resolution of approximately 0.13 μm. Figure 7 shows the only solution found by the algorithm for both the 4 and 60 Kelvin measurements. There is a strong physical agreement between both solutions, with good correspondence of peak positions and peak shape similarity between the 4 and 60 Kelvin measurements. The 4 Kelvin sample shows a significantly larger total current crossing the boundary which is consistent with the variation of the critical cur-
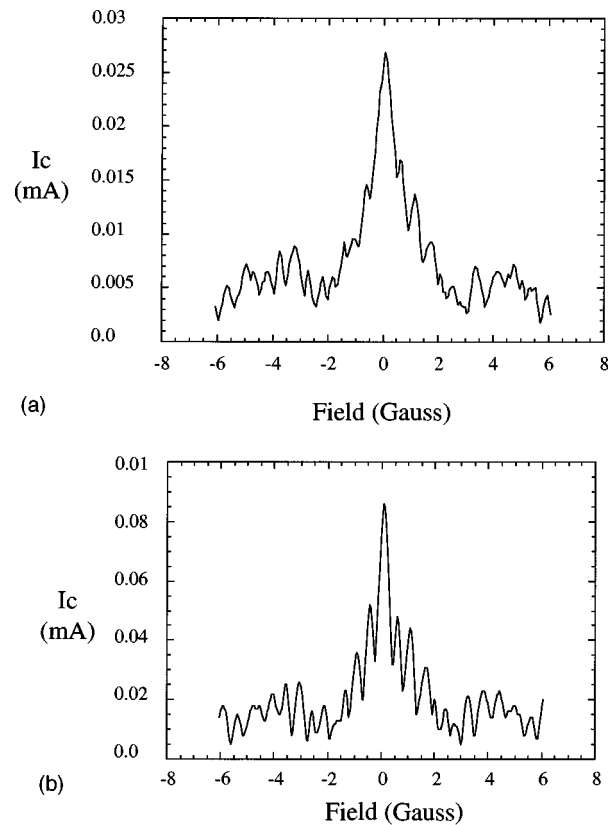
rent with temperature. The results of Fig. 7 indicate that by calculating the positional critical current $J(x)$ as a function of temperature $J(x,T)$, it may be possible to map specific areas along the boundary that have a different superconducting to normal transition temperature than that of the averaged total grain boundary transition temperature. Also, the current distribution at two different temperatures should be similar as in Fig. 7. Thus any solutions found at an intermediate temperature must also conform to the same physical current distribution. Therefore, if there were actually physically different solutions, it would be possible by performing these
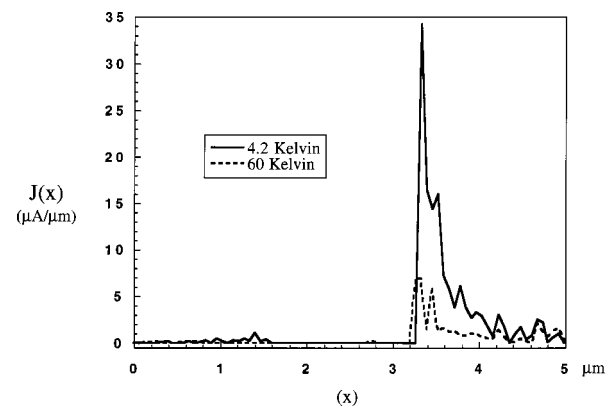

FIG. 7. Positional current density $J(x)$ calculation at 4 and 60 Kelvin calculated from data in Fig. 6.

measurements at various temperatures to eliminate ''nonphysical'' current distributions and determine a unique solution to the problem.

Our ultimate goal is to correlate these current inhomogeneities to structural and compositional variations along the length of the grain boundary. Small deviations of the current from point to point may be very difficult to distinguish microstructurally. Studies of the oxygen stoichiometry along the length of the boundary have revealed that the oxygen content can vary from point to point along the boundary. This may also account for some variations in the local transport properties, but would be very difficult to quantify experimentally. However, as observed above, large areas along the boundary that carry no current (such as the sample in Fig. 7) are expected to have some microstructural irregularities that are distinguishable and can be directly compared with the positional current $J(x)$ solutions.

V. CONCLUSION

The spatial variation of the critical current across the boundary was determined for several YBCO grain boundary Josephson junctions. Using a phase retrieval algorithm and a genetic algorithm in concert with a ranking scheme that tests the conformity of each solution to the known boundary constraints, we are able to determine one unique or a small set of possible correct solutions. In each boundary for which multiple solutions were found, the deviations between solutions were small thus representing the same physically unique situation within the accuracy of the measurements. For each junction the current distributions were highly nonuniform. In most samples the majority of current was carried across a small number of superconducting regions along the length of the boundary. These results are consistent with existing filamentary models and LTSEM and LSM imaging experiments that have been performed on high T_c grain boundary junctions. We have shown that typical grain boundary junctions are far from perfect regarding their local current carrying capacity. This also explains the large range of critical current values that has been reported in the literature for boundaries of the same macroscopic geometry.

ACKNOWLEDGMENTS

[1] R. Gerdemann, K. D. Husemann, R. Gross, L. Alff, A. Beck, B. Elia, W. Reuter, and M. Siegel, J. Appl. Phys. **76**, 8005 (1994).

[2] G. M. Fisher, B. Mayer, R. Gross, T. Nissel, K.-D. Husemann, R. P. Huebener, T. Freltoft, Y. Shen, and P. Vase, Science **263**, 1112 (1994).

[3] J. Mannhart, R. Gross, R. P. Huebener, P. Chaudhari, D. Dimos, and C. C. Tsuei, Cryogenics **30**, 397 (1990).

[4] Y. Y. Divin, H. Schulz, U. Poppe, N. Klein, K. Urban, P. M. Shadrin, I. M. Kotelyanski, and E. A. Stepantsov, Physica C **256**, 149 (1996).

[5] P. M. Shadrin and Y. Y. Divin, Physica C **297**, 69 (1998).

[6] B. D. Josephson, Adv. Phys. **14**, 431 (1965).

[7] D. K. Lathrop, B. H. Moeckly, S. E. Russek, and R. A. Buhrman, Appl. Phys. Lett. **58**, 1095 (1991).

[8] B. Mayer, S. Schuster, A. Beck, L. Alff, and R. Gross, Appl. Phys. Lett. **62**, 783 (1993).

[9] C. Sarma, G. Schindler, D. G. Hasse, C. C. Kock, A. M. Saleh, and A. I. Kingon, Appl. Phys. Lett. **64**, 109 (1994).

[10] R. G. Humphreys, J. S. Satchell, J. A. Edwards, N. G. Chew, S. W. Goodyear, M. N. Keene, and S. F. Morgan, IEEE Trans. Appl. Supercond. **3**, 2026 (1993).

[11] R. G. Humphreys, J. S. Satchell, J. A. Edwards, N. G. Chew, S. W. Goodyear, M. N. Keene, and S. F. Morgan, IEEE Trans. Appl. Supercond. **3**, 2026 (1993).

[12] O. M. Froehlich, H. Schulze, A. Beck, B. Mayer, L. Alff, R. Gross, and R. P. Huebener, Appl. Phys. Lett. **66**, 2289 (1995).

[13] S. Schuster, R. Gross, B. Mayer, and R. P. Huebener, Phys. Rev. B **48**, 16172 (1993).

[14] X. Xiu, Q. Lu, S. Wang, Y. Dai, G. Xiong, G. Lian, R. Me, S. Wang, and Z. Gan, Physica C **282–287**, 2409 (1997).

[15] O. M. Froehlich, H. Schulze, A. Beck, R. Gerdemann, B. Mayer, R. Gross, and R. P. Huebener, IEEE Trans. Appl. Supercond. **5**, 2188 (1995).

[16] L. Alff, B. Mayer, S. Schuster, O. Frohlich, R. Gerdemann, A. Beck, and R. Gross, J. Appl. Phys. **75**, 1843 (1994).

[17] A. Beck, A. Stenzel, O. M. Froehlich, R. Gerber, R. Gerdemann, L. Alff, B. Mayer, and R. Gross, IEEE Trans. Appl. Supercond. **5**, 2192 (1996).

[18] H. H. Zappe, Phys. Rev. B **7**, 2535 (1975).

[19] O. Nesher and E. N. Ribak, Appl. Phys. Lett. **71**, 1249 (1997).

[20] A. Levi and H. Stark, *Image Recovery: Theory and Application, Restoration from Phase and Magnitude by Generalized Projections* (Academic, New York, 1987), p. 277.

[21] M. Carmody, E. Landree, L. D. Marks, and K. L. Merkle, Physica C **315**, 145 (1999).

[22] P. A. Rosenthal, M. R. Beasley, K. Char, M. S. Colclough, and G. Zaharchuck, Appl. Phys. Lett. **59**, 3482 (1991).

[23] D. Robbes, M. Lam Chok Sing, V. Martin, F. Gire, D. Bloyet, N. Quellec, J. Certenais, K. Bouzehouane, D. Dubreuil, and D. Crete, Inst. Phys. Conf. Ser. **148**, 1279 (1995).

[24] R. G. Humphreys and J. A. Edwards, Physica C **210**, 42 (1993).

[25] V. Martin, M. Lam Chok Sing, D. Bloyetr D. Robbes, J. Certenais, N. Quellec, and D. Crete, IEEE Trans. Appl. Supercond. **7**, 3079 (1997).

[26] R. Unger, T. A. Scherer, W. Jutzi, Z. G. Ivanov, and E. A. Stepantsov, Physica C **241**, 316 (1995).

[27] R. I. Joseph and E. Schlomann, J. Appl. Phys. **36**, 1579 (1965).

[28] B. H. Moeckly and K. Char, Physica C **265**, 263 (1997).

[29] B. H. Moeckly and K. Char (unpublished).

[30] B. H. Moeckly and R. A. Buhrman, Appl. Phys. Lett. **65**, 3126 (1994).

[31] B. H. Moeckly and R. A. Buhrman, IEEE Trans. Appl. Supercond. **5**, 3414 (1995).

[32] B. H. Moeckly, D. K. Lathrop, and R. A. Buhrman, Phys. Rev. B **47**, 400 (1993).

[33] E. A. Early, R. S. Steiner, and A. F. Clark, Phys. Rev. B **50**, 9409 (1994).

[34] E. Sarnelli, Interface Sci. **1**, 287 (1993).

[35] E. Sarnelli, P. Chaudhari, and J. Lacey, Appl. Phys. Lett. **62**, 777 (1993).